



Research Article

Analysis and modeling of the thermal behavior of an improved pellet cookstove

Théophile Vitoussia^{1,2} · Alain Brillard³ · Justin Bertsch³ · Olivier Allgaier³ · Gontrand Leyssens³ · Cornélius Schönnebeck³ · Ebenezer Njeugna^{1,2} · Jean-François Brillhac³

Received: 23 November 2020 / Accepted: 4 May 2021

Published online: 20 May 2021

© The Author(s) 2021 OPEN

Abstract

In Sub-Saharan countries, cooking is usually done at a domestic scale using rudimentary stoves with wood or charcoal as combustibles. To improve the cooking behavior and reduce the deforestation, an improved pellet cookstove was conceptualized with guiding ideas in mind such as simplicity, robustness and ability to burn pellets built with local wood residues under a natural draught. Combustion and water ebullition tests were performed with two configurations of the upper part of the cookstove: thick steel plate or ring, and with standardized EN+ pellets as combustible. The main pollutant gases (CO, CO₂ and NO_x), together with O₂, were continuously measured at different positions of the cookstove during a water ebullition test with the ring configuration. The levels measured above the pot were lower than the thresholds currently proposed by the World Health Organization. Simple and phenomenological thermal models were proposed to simulate the plate, or ring, and water temperatures during the combustion or water ebullition tests and to determine the intrinsic convection coefficients. The maximal relative differences between the experimental and simulated temperatures were computed between 7 and 21%. The stove power was evaluated at 4336 ± 23 W. The cookstove yield for the water ebullition test with the ring configuration was computed equal to 12.3 ± 0.1%, slightly lower than that of cookstoves previously analyzed in the literature.

Keywords Improved pellet cookstove · EN+ pellet · Thermal modeling · Water ebullition test · Cookstove yield · Gas concentrations

Abbreviations

C	Carbon contents in the pellets on wet basis, % vol.	$C_{p,r}$	Ring specific heat, 897.5 J kg ⁻¹ K ⁻¹
CO	Carbon oxide in the fume, ppm	$C_{p,wa}$	Water specific heat, 4850.0 J kg ⁻¹ K ⁻¹
CO ₂	Carbon dioxide in the fume, % vol.	C_r	Carbon contents of the residues, 0.045% of mass
$C_{p,fg}$	Specific heat of dry flue gas in standard conditions, J K ⁻¹ m ⁻³	$\frac{dm_{pe}}{dt}$	Pellet mass rate, 0.9/3600 kg s ⁻¹
$C_{p,fgw}$	Specific heat of water vapor in flue gases in standard conditions, J K ⁻¹ m ⁻³	dt	Time increment, s
$C_{p,pl}$	Plate specific heat, 440.0 J kg ⁻¹ K ⁻¹	dT_{pl}	Plate temperature increment, K
$C_{p,po}$	Pot specific heat, 897.5 J kg ⁻¹ K ⁻¹	dT_{po}	Pot temperature increment, K
		dT_r	Ring temperature increment, K
		$F_{b,hole}$	View factor from burner to ring hole, 1.26%
		$F_{b,pl}$	View factor from burner to plate, 6.37%
		$F_{b,r}$	View factor from burner to ring, 5.11%

✉ Alain Brillard, Alain.Brillard@uha.fr | ¹Laboratoire de Mécanique, Université de Douala, B.P 24157, Douala, Cameroun. ²Laboratoire de Mécanique Et de Matériaux Adaptés (LAMMA), Ecole Normale Supérieure D'Enseignement Technique, B.P 1872, Douala, Cameroun. ³Laboratoire Gestion Des Risques Et Environnement (LGRE UR 2334 UHA), Université de Haute-Alsace, 3bis rue Alfred Werner, 68093 Mulhouse, France.



G_d	Actual specific dry flue gas volume, $\text{Nm}^3 \text{kg}^{-1}$	$S_{\text{po,t}}$	Total pot area, 0.3079 m^2
G_w	Actual specific wet flue gas volume, $\text{Nm}^3 \text{kg}^{-1}$	$S_{\text{pl,f}}$	Plate face area, 0.1379 m^2
$h_{e,h}$	Convection coefficient of the horizontal bottom or top face of the pot, $\text{Wm}^{-2} \text{K}^{-1}$	$S_{\text{pl,t}}$	Total plate area, 0.2892 m^2
$h_{e,pl}$	Convection coefficient of the horizontal face of the plate, $\text{Wm}^{-2} \text{K}^{-1}$	$S_{r,f}$	Ring face area, 0.0817 m^2
$h_{e,v}$	Convection coefficient of the vertical face of the pot, $\text{Wm}^{-2} \text{K}^{-1}$	$S_{r,t}$	Total ring area, 0.1797 m^2
H	Hydrogen contents in the pellets on wet basis, % of mass	T_{amb}	Ambient temperature, K
HHV	Pellet Higher Heating Value on raw basis, MJ kg^{-1}	T_a	Ashtray temperature, K
$h_{i,p}$	Convection coefficient (lower face of the plate), $\text{Wm}^{-2} \text{K}^{-1}$	T_b	Burner temperature, K
$h_{i,r}$	Convection coefficient (lower face of the ring), $\text{Wm}^{-2} \text{K}^{-1}$	T_{fl}	Flame temperature, K
k_e	Global heat transfer coefficient between the higher face of the plate or ring and the bottom of the pot, $\text{Wm}^{-2} \text{K}^{-1}$	T_{fu}	Fume temperature at the exhaust of the cookstove, K
LHV	Pellet Lower Heating Value on dry and ash free basis, MJ kg^{-1}	$T_{\text{fu,in}}$	Fume temperature close to the burner, K
M	Moisture contents in the pellets, % of mass	$T_{\text{fu,out}}$	Fume temperature close to the lower face of the plate or ring, K
m_{pl}	Plate weight, 10.95 kg	T_{pl}	Plate temperature, K
m_{po}	Pot weight, 1.50 kg	T_{po}	Pot temperature, K
m_r	Ring weight, 8.79 kg	T_r	Ring temperature, K
m_{wa}	Water weight, 5.0 kg	Greek Letters	
NA	Avogadro number, $6.02 \times 10^{23} \text{ mol}^{-1}$	ϵ_a	Ashtray emissivity, 0.9
NO	Nitrogen oxide in the fume, ppm	ϵ_b	Burner emissivity, 0.9
NO ₂	Nitrogen dioxide in the fume, ppm	ϵ_{fl}	Flame emissivity, 0.4
O ₂	Oxygen in the fume, % of mass	ϵ_{pl}	Plate emissivity, 0.85
$P_{c,r}$	Power associated with convection from the ring, W	ϵ_{po}	Pot emissivity, 1.0
P_{fu}	Power associated with heat losses in the flue gas, W	ϵ_r	Ring emissivity, 0.85
$P_{\text{fu,l}}$	Power associated with latent heat losses in the fume, referred to the pellet unit mass, W	ϕ_{fu}	Fume flow, $\text{Nm}^3 \text{ s}^{-1}$
$P_{\text{fu,s}}$	Power associated with sensitive heat losses in the fume, referred to the pellet unit mass, W	σ	Stefan-Boltzmann constant, $5.67 \times 10^{-8} \text{ Wm}^{-2} \text{ K}^{-4}$
$P_{r,a}$	Power associated with heat losses by downwards radiation from the ashtray, W	η	Cookstove yield, %
$P_{r,b}$	Power associated with heat losses by upwards radiation from the burner, W		
P_{tot}	Cookstove power, W		
Q_a	Sensitive heat losses in the flue gas per unit fuel kilogram, kJ kg^{-1}		
Q_{pe}	Pellet heat, J		
Q_{wa}	Water heat, J		
r_b	Burner radius, 0.06 m		
r_{pl}	Plate radius, 0.18 m		
S_a	Ashtray area, 0.0113 m^2		
S_b	Burner area, 0.0113 m^2		
S_{hole}	Ring hole area, 0.0201 m^2		
$S_{\text{po,h}}$	Bottom pot area, 0.0616 m^2		
$S_{\text{po,v}}$	Lateral pot area, 0.2463 m^2		

1 Introduction

In Sub-Saharan countries, cooking is usually done at a domestic scale using rudimentary stoves among which the most familiar is the three-stone one [26]. People here mainly use charcoal, wood residue or biomass as combustible. The efficiency of such low-cost stoves is quite poor, the main pollutant gaseous (CO, CO₂ and NO_x) and particulate emissions occurring during combustion are quite high, and the use of charcoal or of raw wood as combustible contributes to deforestation [17]. To increase the efficiency and to reduce the pollutant gaseous and particulate emissions, improved stoves are being designed. Following [18], an improved cookstove is “a cookstove designed using certain scientific principles, to assist better combustion and heat transfer, for improving emissions and efficiency performance”. A classification of improved cookstoves is proposed in [23]. Such improved cookstoves should have a power and an efficiency greater than that of traditional ones. To limit deforestation, combustible for cooking purpose or heat production at a domestic scale should be produced from forest- or agro-industrial waste, which may further be first assembled in pellets for an easier transportation from the

production zone to the use zones and even during the use in domestic cookstoves. Pelletization also leads to an increase of the energetic density that allows transporting more energy density per volume. From an economic point of view, the paper [15] analyzes the development of a firm producing biomass pellets in Rwanda and selling an improved cookstove to reduce the use of charcoal. The amount of pellets required for different cooking preparations was also evaluated in this paper. In the paper [20], the authors carried out an economic assessment of a gasification-based wood gas stove designed for a six-member family and burning babul wood and groundnut shell pellet under natural or forced draught.

In the present study, a low-cost prototype of improved pellet cookstove was designed at a lab scale for wood pellet combustion. Combustion tests were performed in the cookstove with a thick steel plate on its top. Water ebullition experiments were performed with the plate or with a thick steel ring on the top of the cookstove. To perform such water ebullition tests, whose protocol is described in the review [21] and in the references therein, a pot containing 5 L of water was posed on the plate or ring. The initial temperature of the water was the ambient one, thus leading to a so-called cold-start water ebullition test. The combustion or water ebullition tests were performed outdoor, but in a zone sheltered from wind, to mimic the domestic conditions of Sub-Saharan cooking. Although the prototype was designed for cooking purpose in Sub-Saharan countries with pellets made with local woody waste, the combustion and water ebullition tests were performed with standardized EN+ pellets. These pellets were manually and periodically injected in the combustion zone to maintain a high combustion level during the test. For both tests, the temperatures were continuously recorded along the experiment at different positions of the cookstove. The main pollutant gases (CO, CO₂ and NO_x), together with O₂, were continuously recorded at different positions of the cookstove. Simple and phenomenological heat transfer models were proposed to simulate the plate, or ring, and water temperatures along the combustion or water ebullition tests. They involve parameters which were computed in terms of some experimental temperatures and gas concentrations, and convection coefficients. These intrinsic convection coefficients were determined comparing the experimental and simulated temperatures. The cookstove power, some of its components, and the stove yield were finally computed, using the standards NF EN 16510 [5]. Differences between the values of these parameters and physical quantities obtained in the present study appear with that of the literature, see [6, 10, 14, 20, 31, 32], and [33], for example, see also the review [11] and the references in these papers. These differences may be explained by differences in the conception of the

cookstove, its draught, and in the combustibles which are used for the experimental tests.

2 Materials and methods

2.1 Description of the improved pellet cookstove

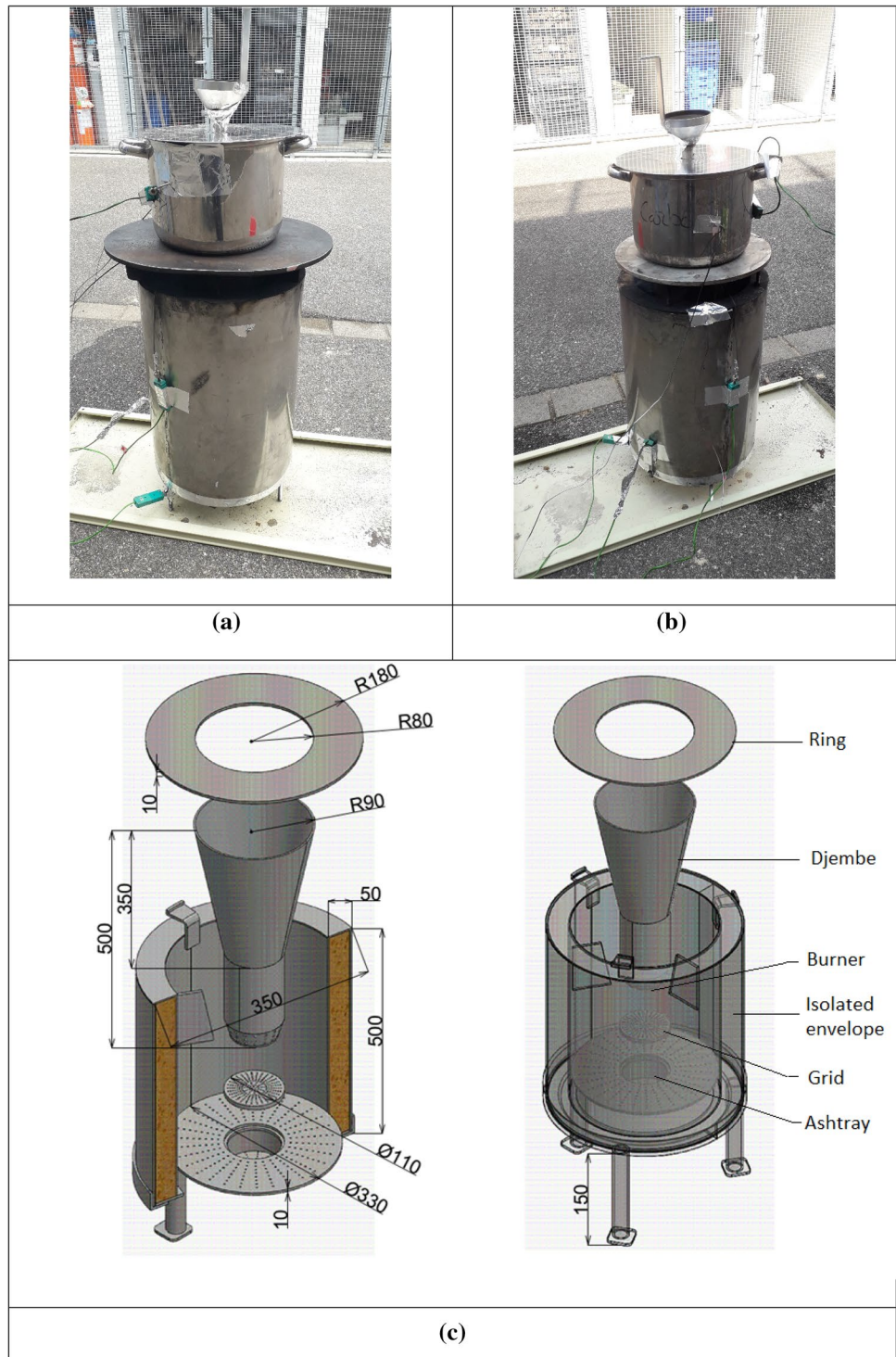
The low-cost prototype of improved pellet cookstove was designed in Douala, Cameroon, and manufactured in Mulhouse, France. It may be characterized by:

- A circular shape, for an easier manufacturing;
- A conical shape of the burner to concentrate the circulation of the heat flux and of the fume to the plate or ring;
- A free space between the djembe and the inner envelope, which builds a first insulating layer;
- An insulating material between the two envelopes of the lateral face of the cookstove, to prevent the user from hot temperatures;
- A cookstove height which allows cooking at human height;
- A combustion realized under natural draught;
- The use of pellets made with local forest- and agro-industrial waste as combustible, to limit deforestation.

Figure 1 presents photographs of the cookstove with the thick plate or the thick ring on its upper part and a scheme of this cookstove with the ring on its upper part.

The present study focuses on the analysis of the cookstove behavior with two configurations: a thick steel plate, see Fig. 1 a), or with a thick steel ring placed on its upper part, Fig. 1 b). The central part of the cookstove consists of a unique metallic piece obtained when welding a cone to a cylinder to get the shape of a musical instrument called djembe. The lower cylindrical part of the djembe has a diameter equal to 15 cm and a height of 9.5 cm. Its higher part ends with a diameter equal to 18 cm and has a height equal to 30.5 cm. The lower cylindrical part of the djembe is perforated on its lateral surface to bring a secondary airflow to the burner zone. The base of the burner is put on a thick metallic grid where the pellets are burnt. During the combustion, ash falls in an ashtray through the grid perforated with holes of diameter 2 mm. The thickness of the metallic grid is equal to 6 mm to increase its resistance to heat and to maintain the embers on a sufficiently long time length at high temperatures, thanks to an inertia effect. The upper cylindrical part of the djembe is designed to drive the hot fume to the upper part of the cookstove. A free space of approximately 5 cm is maintained between the upper edge of the djembe and the plate or ring, to

Fig. 1 Photographs of the improved cookstove with the plate (a) or ring (b) configurations, and 3D scheme (c) of the improved pellet cookstove with the thick ring



let the fume leave the combustion zone after licking this plate or ring. The thick plate has a radius equal to 0.18 m and a thickness equal to 0.01 m. A small hole is perforated in the center of the plate to periodically inject the pellets in the combustion zone. The feeding system is visible in Fig. 1 a) and b) on the top of the cookstove equipped for a water ebullition test, here with the plate.

The configuration with a ring was motivated observing that when performing a water ebullition test with the plate configuration, the water temperature never reached 100 °C. On the contrary, when putting the pot on the ring, the water temperature was able to reach 100 °C after 2310 s. The cookstove was insulated along its lateral surface to protect the user during the combustion

or water ebullition tests. The height of the cookstove was equal to 0.50 m and that of the support was equal to 0.15 cm.

2.2 EN+ pellet characterizations

Even if the cookstove was intended to burn pellets made with Cameroonian local forest- or agro-industrial waste, standardized EN+ pellets were used as combustible during the combustion and water ebullition tests, which were considered at a lab scale in the present study. The EN+ certification refers to the European standards NF EN 17225-2 [3], concerning the production of industrial and non-industrial pellets.

The ultimate analysis of the EN+ pellets was performed with an automatic elemental analyzer (EuroVector EA-3000) and according to ISO 29541 [2], ISO 19579 [1], and ASTM 3176-15 [12] standards. Carbon (C), Hydrogen (H), Nitrogen (N) and Sulfur (S) contents were measured and the oxygen content (O) was deduced from the overall balance. The ultimate analysis was based on the sample combustion, followed by separation in a gas chromatography column and detection of the combustible products using a high sensitive catharometric detector. The atomic ratios H/C and O/C were calculated according to Van Krevelen's biomass formulas [27]:

$$H/C = \frac{\frac{\%H}{1/NA}}{\frac{\%C}{12/NA}}; O/C = \frac{\frac{\%O}{16/NA}}{\frac{\%C}{12/NA}} \quad (1)$$

where %H, %C and %O are the percentages of H, C and O determined in the ultimate analysis and NA is the Avogadro number ($NA = 6.02 \cdot 10^{23}$ atoms per mol).

The proximate analysis of the EN+ pellets was performed using standard techniques and according to ISO 1171 (2015) and NF EN ISO 18122 [4] standards for biomass samples. The moisture content was determined by placing the sample in a Memmert VM400 oven at 105 ± 2 °C for 24 h, the sample mass remaining almost constant after this time length. A Nabertherm muffle furnace was used to determine the ash content of EN+ pellets at 550 °C or 815 °C, according to NF EN ISO 18122 [4].

The higher heating value (HHV) of the EN+ pellets was determined placing the raw sample in a metal crucible (accuracy 0.1 mg) in a calorimeter IKA C200. Three measures of the HHV were performed. The lower heating value (LHV) was deduced from the HHV, according to the formula:

$$LHV = HHV - L_v \left(\frac{M}{100} + \frac{M_{H_2O}H}{200M_H} \right), \quad (2)$$

where $L_v = 2486$ kJ.kg⁻¹ is the latent heat of water vaporization at 273 K, M is the moisture content (%) determined

in the proximate analysis, $M_{H_2O} = 18$ g.mol⁻¹ is the water molar mass, $M_H = 1$ g.mol⁻¹ is the hydrogen molar mass and H is the percentage of hydrogen in the sample determined in the ultimate analysis. A corrected lower heating value was finally computed on dry and ash-free material through the formula:

$$LHV_{daf} = LHV \times \frac{100}{100 - Ash_{550}}, \quad (3)$$

where Ash_{550} is the ash percentage determined at 550 °C.

2.3 Combustion and water ebullition tests

Combustion tests were performed with the plate configuration. Water ebullition tests were performed with the thick plate or ring configurations. For these water ebullition tests, a pot with radius 14 cm and height 28 cm was filled with 5 L water and put on the plate or ring. A lid was placed on the top of the pot during this water ebullition test.

Whatever the test, the ignition was performed using a natural cubic fire starter, which was inserted into the fire-place with a thin layer of pellets. The amount of pellets inserted for ignition was weighed, and this amount was included in the total consumption of pellets per hour.

Figure 2 presents photographs of the pot placed on the top face of the plate or ring, for a water ebullition test.

Because the bottom of the pot covers the central part of the plate or ring, a tube was welded in the center of the internal bottom face of the pot to inject pellets in the combustion zone of the cookstove during a water ebullition test. The tube was long enough to come over the perforated lid placed on the top of the pot, see Fig. 1 a). The plate was also perforated in its central part with a small hole placed just under the tube, in the case of water ebullition test. Pellets were injected by hand in the combustion zone of the cookstove through the plate hole or the pot tube: 0.9 kg of pellets were periodically injected (approximately 10 pellets every 30 s) during the combustion or water ebullition tests, whose time length was approximately equal to 2 h.



Fig. 2 The pot to be put on the plate or ring and which was perforated by a tube in its center, to periodically inject the pellets in the combustion zone

To mimic the combustion performed in Sub-Saharan houses, the combustion or water ebullition tests were carried outside, but in a zone sheltered from wind. They were repeated at least three times with good repeatability, at least for the plate, or ring, and water temperature.

2.4 Temperature measurements

During the combustion or water ebullition tests, temperatures were continuously measured along the experiment at different positions of the system: on the ashtray, lower grid, plate or ring, along the pot walls, inside the fume and the water, through K-type thermocouples (maximal temperature 1370 °C, accuracy ± 2.2 °C), see Fig. 1 a) and b) for the positions of some thermocouples. The ambient temperature T_{amb} was also continuously measured.

2.5 Main gas concentrations

During a water ebullition test, the main gases (CO, NO_x, CO₂, and O₂) were measured using a portable TESTO 350-XL fume analyzer and a probe. These concentrations were measured every second along the water ebullition test and during approximately 10 min. The CO, CO₂, and O₂ concentrations measured in the center of the combustion zone will be used for the determination of the cookstove power and yield.

The accuracy of the gaseous concentration measurements is equal to ± 5% for CO, ± 5 ppm for NO_x, ± 1.3% for CO₂ and ± 0.2 vol. % for O₂, in the present experimental conditions.

2.6 Heat transfer models

2.6.1 System burner + plate

The thermal balance of the system burner + plate is written according to [16], as:

$$h_i S_{pl,f} (T_{fu}(t) - T_{pl}(t)) dt + F_{b,pl} \epsilon_{fl} S_b \sigma T_{fl}^4(t) dt = h_{e,pl} S_{pl,f} (T_{pl}(t) - T_{amb}(t)) dt + S_{pl,t} \epsilon_{pl} \sigma T_{pl}^4(t) dt + m_{pl} C_{p,pl} dT_{pl}(t), \tag{4}$$

where the left-hand side corresponds to the gains for the system through the convection from the fume and through the flame radiation from the burner. The right-hand side of (4) corresponds to the losses through the convection in the ambient atmosphere on the upper surface

$$h_i S_{pl,f} (T_{fu}(t) - T_{pl}(t)) dt + F_{b,pl} \epsilon_{fl} S_b \sigma T_{fl}^4(t) dt = h_{e,pl} (S_{pl,f} - S_{po,h}) (T_{pl}(t) - T_{amb}(t)) dt + (S_{pl,t} - S_{po,h}) \epsilon_{pl} \sigma T_{pl}^4(t) dt + k_e S_{po,h} (T_{pl}(t) - T_{po}(t)) dt + m_{pl} C_{p,pl} dT_{pl}(t), \tag{7}$$

of the plate, the radiation from the total plate surface, during dt , and the temperature increase of the plate.

In [22], a more elaborated heat transfer model was proposed for a cookstove with a different shape.

The definition of the different parameters appearing in Eq. (4) and some of their values are indicated in the Abbreviations.

The thermal balance (4) may be written as the differential equation:

$$\frac{dT_{pl}}{dt}(t) = \frac{1}{m_{pl} C_{p,pl}} \left(h_i S_{pl,f} (T_{fu}(t) - T_{pl}(t)) + F_{b,pl} \epsilon_{fl} S_b \sigma T_{fl}^4(t) - h_{e,pl} S_{pl,f} (T_{pl}(t) - T_{amb}(t)) - S_{pl,t} \epsilon_{pl} \sigma T_{pl}^4(t) \right). \tag{5}$$

The plate temperature T_{pl} starts from the initial ambient temperature $T_{amb}(0)$ at $t=0$.

The differential Eq. (5) involves the unknown convection coefficients h_i and $h_{e,pl}$ to be determined through a comparison between the experimental and simulated plate temperatures. The differential Eq. (5) is indeed solved using Scilab software and the explicit Euler method, first with initial guesses of the unknown convection coefficients h_i and $h_{e,pl}$. Then the Scilab routine 'data-fit' is applied, which consists to minimize the sum over the experiment times of the squared difference between the experimental and simulated plate temperatures:

$$\sum_{j=1}^J (T_{pl,exp}(j) - T_{pl,sim}(j))^2, \tag{6}$$

where J is the overall number of experimental time points, $T_{pl,exp}(j)$ the experimental plate temperature at time t_j , and $T_{pl,sim}(j)$ the simulated plate temperature at time t_j . Equation (5) is finally solved with the optimal values of the convection coefficients h_i and $h_{e,pl}$.

2.6.2 System burner + plate + pot + water

The thermal balance of the system burner + plate + pot + water consists of the two following equations:

$$\begin{aligned}
 k_e S_{po,h} (T_{pl}(t) - T_{po}(t)) dt &= h_{e,v} S_{po,v} (T_{po}(t) - T_{amb}(t)) dt \\
 &+ h_{e,h} S_{po,h} (T_{po}(t) - T_{amb}(t)) dt + \epsilon_{po} S_{po,t} \sigma T_{po}^4(t) dt \\
 &+ (m_{po} C_{p,po} + m_{wa} C_{p,wa}) dT_{po}(t).
 \end{aligned} \tag{8}$$

In the balance Eq. (7), the left-hand side gathers the gain terms for the system through either the convection from the fume or the flame radiation from the burner, during dt . The right-hand side of (7) represents the losses through either the convection from the part of the plate surface not covered by the pot, the radiation from the plate surface not covered by the pot, the heat exchange between the plate and the pot, during dt , and the temperature increase of the plate.

The optimal values of the convection coefficients h_i and $h_{e,pl}$ are taken from the previously described computations concerning the combustion test with the plate configuration. Equation (7) involves a further global heat transfer coefficient k_e between the higher face of the plate and the bottom of the pot, which has to be determined.

In the balance Eq. (8), the left-hand side corresponds to the gain through the convection from the plate, during dt . The right-hand side corresponds to the losses through convection along the vertical pot surface and along the lid, the radiation from the pot, during dt , and the temperature increase of the pot and water. The pot and water are indeed supposed to be at a same temperature.

Equation (8) involves two further unknown convection coefficients $h_{e,h}$ and $h_{e,v}$. The lid and vertical face of the pot are indeed separated, both being in contact with the surrounding air.

The definition of the parameters involved in the balance Eqs. (7)-(8) and some of their values are indicated in the

$$\begin{aligned}
 h_i S_{r,f} (T_{fu}(t) - T_r(t)) dt + F_{b,r} \epsilon_{fl} S_b \sigma T_{fl}^4(t) dt &= h_{e,pl} (S_{r,f} - S_{po,h}) (T_r(t) - T_{amb}(t)) dt \\
 &+ (S_r - S_{po,h}) \epsilon_r \sigma T_r^4(t) dt \\
 &+ k_e (S_{po,h} - S_{hole}) (T_r(t) - T_{po}(t)) dt \\
 &+ m_r C_{p,r} dT_r(t),
 \end{aligned} \tag{12}$$

Abbreviations.

The system (7)-(8) of balance equations may be written as the coupled system of differential equations:

$$\frac{dT_{pl}(t)}{dt} = \frac{1}{m_{pl} C_{p,pl}} \left(\begin{array}{l} h_i S_{pl,f} (T_{fu}(t) - T_{pl}(t)) + F_{b,pl} \epsilon_{fl} S_b \sigma T_{fl}^4(t) \\ -h_{e,pl} (S_{pl,f} - S_{po,h}) (T_{pl}(t) - T_{amb}(t)) \\ -(S_{pl,t} - S_{po,h}) \epsilon_{pl} \sigma T_{pl}^4(t) - k_e S_{po,h} (T_{pl}(t) - T_{po}(t)) \end{array} \right), \tag{9}$$

$$\frac{dT_{po}(t)}{dt} = \frac{1}{m_{po} C_{p,po} + m_{wa} C_{p,wa}} \left(\begin{array}{l} k_e S_{po,h} (T_{pl}(t) - T_{po}(t)) - h_{e,v} S_{po,v} (T_{po}(t) - T_{amb}(t)) \\ -h_{e,h} S_{po,h} (T_{po}(t) - T_{amb}(t)) - \epsilon_{po} S_{po,t} \sigma T_{po}^4(t) \end{array} \right). \tag{10}$$

The plate temperature T_{pl} and the pot temperature T_{po} both start from the ambient temperature $T_{amb}(0)$ at $t=0$. This leads to a so-called cold-start water ebullition test.

The system (9)-(10) of differential equations is solved using the Scilab software and the explicit Euler method, first with initial guesses of the unknown parameters k_e , $h_{e,h}$ and $h_{e,v}$. The optimal values of these parameters k_e , $h_{e,h}$ and $h_{e,v}$ are determined applying the Scilab optimisation routine 'datafit', which consists to minimize the sum over the experiment times of the squared differences between the experimental and simulated plate and pot temperatures:

$$\sum_{j=1}^J \left((T_{pl,exp}(j) - T_{pl,sim}(j))^2 + (T_{po,exp}(j) - T_{po,sim}(j))^2 \right), \tag{11}$$

where J is the overall number of experiment times, $T_{po,exp}(j)$ the experimental water temperature at time t_j , and $T_{po,sim}(j)$ the simulated water temperature at time t_j . The system (9)-(10) is finally solved with the optimal values of the parameters k_e , $h_{e,h}$ and $h_{e,v}$.

2.6.3 System burner + pot + water in the ring configuration

The thermal balance of the system burner + ring + pot + water is composed of the two equations:

$$\begin{aligned}
 k_e(S_{po,h} - S_{hole})(T_r(t) - T_{po}(t))dt + h_i S_{hole}(T_{fu}(t) - T_{po}(t))dt + F_{b,hole} \epsilon_{fl} S_b \sigma T_{fu}^4(t)dt = h_{e,v} S_{po,v}(T_{po}(t) - T_{amb}(t))dt \\
 + h_{e,h} S_{po,f}(T_{po}(t) - T_{amb}(t))dt \\
 + \epsilon_{po} S_{po,t} \sigma T_{po}^4(t)dt \\
 + (m_{po} C_{p,po} + m_{wa} C_{p,wa}) dT_{po}(t).
 \end{aligned} \tag{13}$$

In the balance Eq. (12), the first term of the left-hand side corresponds to the heat brought from the fume to the ring during dt and the second term corresponds to the radiation from the burner to the ring during dt . The first term of the right-hand side corresponds to the heat lost by the portion of the ring not covered by the pot to the air, the second term corresponds to the radiation from this portion of the ring, the third term corresponds to the transfer from the portion of the ring covered by the pot to this pot, during dt , and the fourth term corresponds to the increase of the ring temperature.

In the balance Eq. (13), the first term of the left-hand side corresponds to the heat brought by the portion of the ring covered by the pot to this pot, the second term corresponds to the heat brought by the fume directly to the pot through the ring hole, and the third term corresponds to the radiation from the burner through the ring hole, during dt . The first term of the right-hand side of the balance Eq. (13) corresponds to the loss from the pot the ambient air through the vertical face of the pot, the second term corresponds to the loss from the lid, the third term corresponds to the radiation from the free surface of the pot, during dt , and the fourth term corresponds to the heat increase of the pot + water.

The system (12)-(13) of balance equations may be written as the coupled system of two differential equations:

$$\frac{dT_r(t)}{dt} = \frac{1}{m_r C_{p,r}} \begin{pmatrix} h_i S_{r,f}(T_{fu}(t) - T_r(t)) + F_{b,r} \epsilon_{fl} S_b \sigma T_{fl}^4(t) \\ -h_{e,r}(S_{r,f} - S_{po,h})(T_r(t) - T_{amb}(t)) \\ -(S_r - S_{po,h}) \epsilon_{pl} \sigma T_r^4(t) - k_e(S_{po,h} - S_{hole})(T_r(t) - T_{po}(t)) \end{pmatrix}, \tag{14}$$

$$\frac{dT_{po}(t)}{dt} = \frac{1}{m_{po} C_{p,po} + m_{wa} C_{p,wa}} \begin{pmatrix} k_e(S_{po,h} - S_{hole})(T_r(t) - T_{po}(t)) \\ + h_i S_{hole}(T_{fu}(t) - T_r(t)) \\ + F_{b,hole} \epsilon_{fl} S_b \sigma T_{fu}^4(t) - h_{e,v} S_{po,v}(T_{po}(t) - T_{amb}(t)) \\ - h_{e,h} S_{po,h}(T_{po}(t) - T_{amb}(t)) - \epsilon_{po} S_{po,t} \sigma T_{po}^4(t) \end{pmatrix}. \tag{15}$$

The ring temperature $T_r(t)$ and the pot temperature T_{po} both start from the initial ambient temperature $T_{amb}(0)$ at $t=0$. The system (14)-(15) is solved using the Scilab software and the explicit Euler method, first with initial guesses of the unknown parameters $k_e, h_{e,r}, h_i, h_{e,h}$ and $h_{e,v}$. The optimal values of these parameters $k_e, h_{e,r}, h_i, h_{e,h}$ and $h_{e,v}$ are determined applying the Scilab optimisation

routine 'datafit', which consists to minimize the sum over the experiment times of the squared differences:

$$\sum_{j=1}^J \left((T_{r,exp}(j) - T_{r,sim}(j))^2 + (T_{po,exp}(j) - T_{po,sim}(j))^2 \right), \tag{16}$$

between the experimental and simulated ring and pot temperatures. The system (14)-(15) is finally solved with the optimal values of the parameters $k_e, h_{e,r}, h_i, h_{e,h}$ and $h_{e,v}$.

2.7 Cookstove power and yield, specific fuel consumption

The cookstove power P_{tot} is evaluated during a water ebullition test with the ring configuration, through the expression:

$$P_{tot} = \frac{dm_{pe}}{dt} \times LHV, \tag{17}$$

where $\frac{dm_{pe}}{dt}$ is the mass rate of injected pellets during the experiment and LHV is the lower heating value of the pellets, to also take into account the latent heat of water vaporization during the pellet combustion.

The power produced during the water ebullition experiment is partly transmitted to the ring + pot + water system and partly lost by convection, radiation, or in the fume [28], as expressed in the following formulas:

The power $P_{r,b}$ corresponding to upwards radiation from the burner is computed through:

$$P_{r,b} = \epsilon_b S_b \sigma T_b^4 \tag{18}$$

The power $P_{r,a}$ associated with the heat losses by downwards radiation from the ashtray is computed through:

$$P_{r,a} = \epsilon_a S_a \sigma T_a^4 \tag{19}$$

The power $P_{fu,s}$ associated with the sensitive heat losses in the fume is computed through:

$$\begin{cases} P_{fu,s} = \frac{Q_a \times \text{pellet flow}}{3600} \\ Q_a = (T_{fu,out} - T_{amb}) \left[\frac{C_{p,fg}(C - C_r)}{0.536(CO + CO_2)} + C_{p,fgw} 1.244 \frac{9H+M}{100} \right], \end{cases} \tag{20}$$

where:

Q_a represents the sensitive heat losses in the flue gas, $T_{fu,out}$ is the fume temperature (K) close to the lower surface of the ring,

C is the carbon contents of the pellet (% on wet basis),

C_r is the carbon contents of the residue (%),

CO is the CO concentration,

CO_2 is the CO_2 concentration in the combustion zone,

$C_{p,fgw}$ is the specific heat of water vapor in flue gases in standard conditions,

H is the hydrogen contents of the pellet (% on wet basis),

M is the moisture contents of the pellet (%).

The constant 1.244 is the specific volume of water vapor, which is given in the standards EN 16510 [5] as: $v_{mol}/M_{H_2O} = 22.414/18.01528 \text{ m}^3 \cdot \text{kmol}^{-1} / (\text{kg} \cdot \text{kmol}^{-1}) = 1.244 \text{ m}^3 \cdot \text{kg}^{-1}$, as proposed in the European standards NF-EN 16510-1 [5].

The power $P_{fu,l}$ associated with the latent heat in the fume is computed through:

$$P_{fu,l} = \frac{12644 \times CO(C - C_r)}{0.536 \times (CO + CO_2) \times 100} \tag{21}$$

In the computations of the expressions (18)-(21) of the different losses, mean values of the concentrations measured in the center of the combustion zone and of the temperatures will be used, thus assuming a “permanent” regime.

The specific heats $C_{p,fg}$ and $C_{p,fgw}$ present in the formula (20) depend on the fume temperature $T_{fu,out}$, measured close to the lower face of the ring and here expressed in °C, and on the CO_2 concentration according to the following formulas [5]:

$$C_{p,fg} = 3.6 \left(0.361 + 0.008 \frac{T_{fu,out}}{1000} + 0.034 \left(\frac{T_{fu,out}}{1000} \right)^2 + \left(0.085 + 0.19 \frac{T_{fu,out}}{1000} - 0.14 \left(\frac{T_{fu,out}}{1000} \right)^2 \right) \frac{CO_2}{100} + \left(0.03 \frac{T_{fu,out}}{1000} - 0.2 \left(\frac{T_{fu,out}}{1000} \right)^2 \right) \left(\frac{CO_2}{100} \right)^2 \right) \tag{22}$$

$$C_{p,fgw} = 3.6 \left(0.414 + 0.038 \frac{T_{fu,out}}{1000} + 0.034 \left(\frac{T_{fu,out}}{1000} \right)^2 \right) \tag{23}$$

Considering the water ebullition test performed in the ring configuration, the cookstove yield may be computed as the ratio between the overall energy required to bring the water contained in the pot to ebullition (100 °C) to that brought from the pellet combustion:

$$\eta = \frac{Q_{wa}}{Q_{pe}} = \frac{m_{wa} \times C_{p,wa} \times (100 - T_{amb})}{m_{pe} \times HHV} \tag{24}$$

The specific fuel consumption is finally computed as the ratio between the amount of combustible required to bring the water contained in the pot to ebullition and the water mass m_{wa} . It is measured in kilograms of combustible per kilograms of water.

Table 1 Ultimate analysis, H/C and O/C ratios, proximate analysis, HHV and LHV, for the EN+ pellets

Ultimate analysis (%)					H/C ratio		O/C ratio
C	H	O	N	S			
47.1	6.1	46.6	<0.1	<0.03	1.55		0.74
Proximate analysis (%) as received					HHV MJ/kg ^a	LHV MJ/kg ^a	LHV _{daf} MJ/kg ^b
M	FC	VM	Ash (550 °C)	Ash (850 °C)			
8.0	79.3	2.7	0.3	0.3	18.8	17.3	17.3

^aon raw basis

^bon dry and ash free basis

The actual specific flue gas volume in wet conditions may be calculated through:

$$G_w = \frac{C - C_r}{0.536 \times (CO_2 + CO)} + 1.24 \times \frac{9H + M}{100} \quad (25)$$

and the actual specific dry flue gas volume may be calculated through:

$$G_d = \frac{C - C_r}{0.536 \times (CO_2 + CO)} \quad (26)$$

3 Results and discussion

3.1 EN+ pellet characterizations

The results of the ultimate and proximate analyses are gathered in Table 1.

The sulfur content is lower than the detection limit, which is usual for woody biomass. The H/C and O/C ratios are comparable to that of other biomass [27].

Through three repetitions, the standard deviations of the HHV may be evaluated at $\pm 100 \text{ kJ.kg}^{-1}$.

Fig. 3 Temperatures measured along a combustion test, with the plate configuration, on the ashtray (small hyphens), on the grid (solid line) and on the plate (dotted line), and ambient temperature (large hyphens, secondary axis)

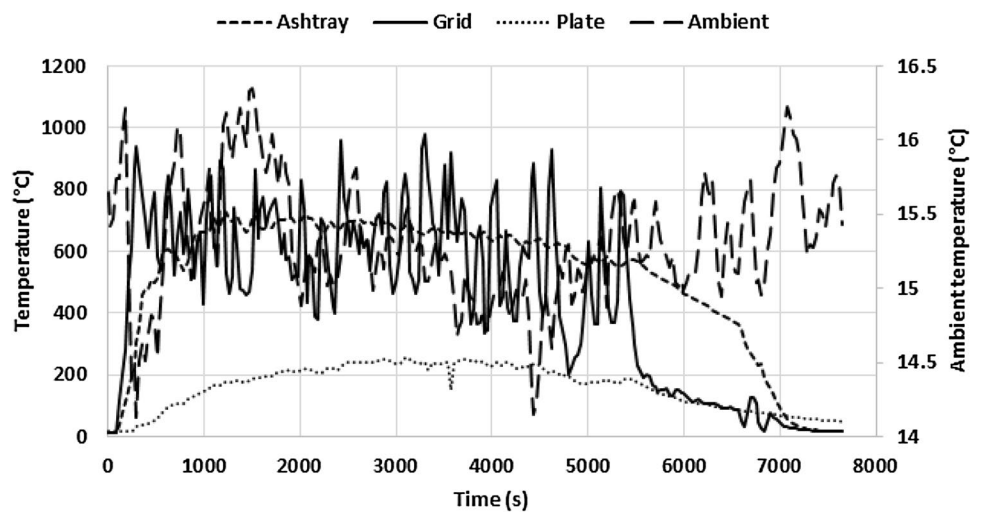
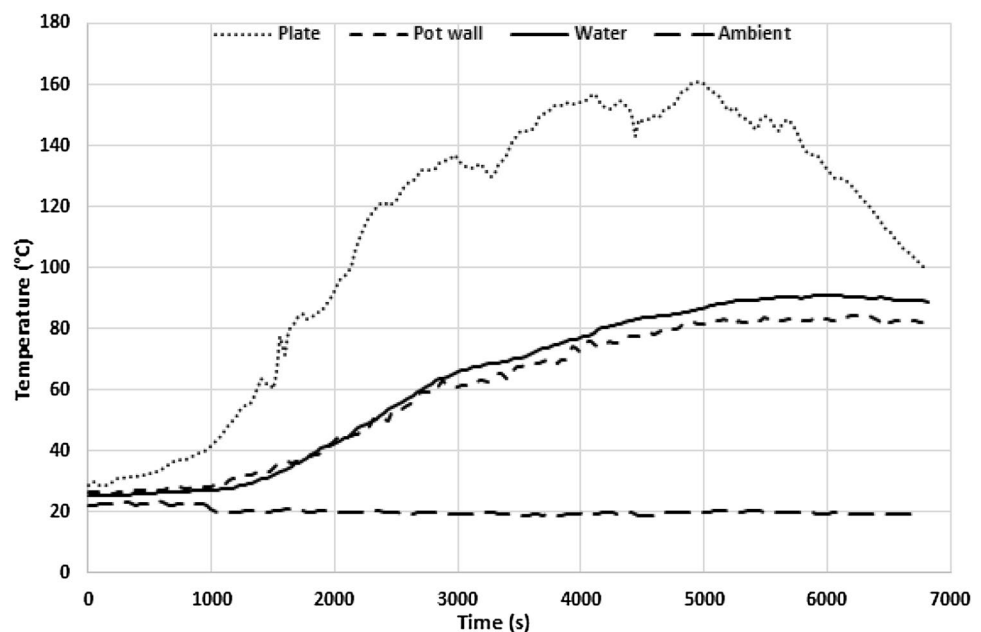


Fig. 4 Temperatures of the plate (dotted line), of the pot wall (solid line), of the water (hyphenated line), and ambient, during a water ebullition test with the configuration of a plate



3.2 Temperature measurements

3.2.1 Combustion test in the plate configuration

During a combustion test with the plate configuration, the temperatures measured at different points of the cookstove present variations gathered in Fig. 3.

The ashtray temperature increases up to approximately 700 °C, where it becomes stable. Then it decreases as soon as no more pellets are being injected in the burner (after 5500 s). The grid temperature increases up to 800 °C, where it starts presenting high oscillations around 600 °C in the central stage of the combustion test. These high fluctuations occur because of the periodic injection of pellets, which perturbs the combustion behavior, whence the heat production. The plate temperature slowly increases up to 230 °C where it remains almost stable during the combustion test. It decreases at the end of the combustion experiment for the above-described reasons. The ambient temperature oscillates between 14 and 16.5 °C.

3.2.2 Water ebullition test in the plate configuration

When a pot containing 5 L of water is placed on the plate, the temperatures of the plate, pot wall, and water inside the pot, measured during a water ebullition test performed with a lid placed over the pot present the shapes exposed in Fig. 4, together with the ambient temperature.

The plate temperature increases up to 120–160 °C, then decreases at the end of the water ebullition test (after 5000 s), for the above-described reasons. The plate temperature is much lower in the presence of a pot containing water than in the absence of pot: 160 versus 230 °C. This is due to the transfer of part of the plate heat to the

pot + water subsystem. The pot wall temperature slowly increases to 80–85 °C. The water temperature slowly increases up to the maximal temperature of 95 °C, which is reached in 1.5 h. The water ebullition temperature of 100 °C is never reached in this configuration with a plate. The ambient temperature remains approximately equal to 20 °C all along the test.

3.2.3 Water ebullition test with the ring configuration

In the configuration with a ring, the temperatures of the fume under the pot, of the pot wall and of the water are gathered in Fig. 5, together with the ambient temperature.

The fume temperature under the pot increases up to 500 °C with high oscillations around this value, because of the discontinuous injection of pellets. The ring temperature increases to 250 °C. The pot wall temperature and the water temperature increase from ambient temperature up to 100 °C and remain very close along the water ebullition test. The ambient temperature is almost constant equal to 36 °C during this water ebullition test with the ring configuration.

The time required for the water to reach ebullition (100 °C) is equal to 2310 s, hence 38.5 min. In [13], the time to ebullition was measured at 31 min for a traditional charcoal cookstove under cold start, at 20 min for a three-stone stove and between 21 and 29 min for improved cookstoves. In [9], the time to ebullition was measured for three improved cookstoves between 64.3 and 72.3 min. In [19], the time to ebullition was estimated between 17 and 22 min, depending on the stove. In [7], the time to ebullition was evaluated at 38 min for in an open air burner with wood. The high differences between these values may be explained by the differences concerning the stove, its

Fig. 5 Fume temperature under the pot (mixed hyphens, principal axis), ring temperature (dotted line, secondary axis), pot wall temperature (small hyphens, secondary axis), water temperature (solid line small hyphen, secondary axis), and ambient temperature (large hyphens, secondary axis), during a water ebullition test, in the configuration with a ring

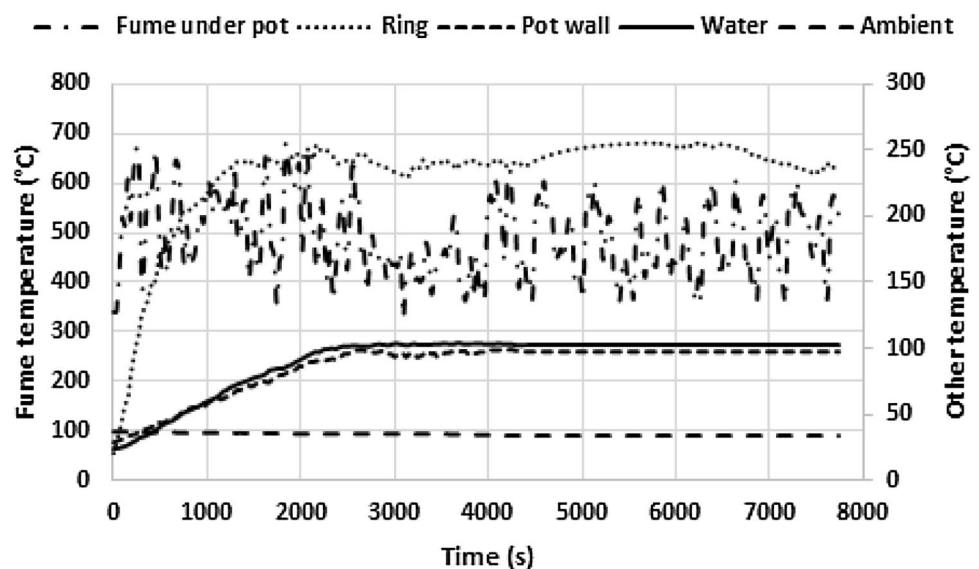


Fig. 6 CO (solid line, ppm, principal axis), NOx (dotted line, ppm, principal axis), CO₂ (small hyphened line, %, secondary axis) and O₂ (large hyphened line, %, secondary axis) emissions during a water ebullition test in the center of the combustion zone

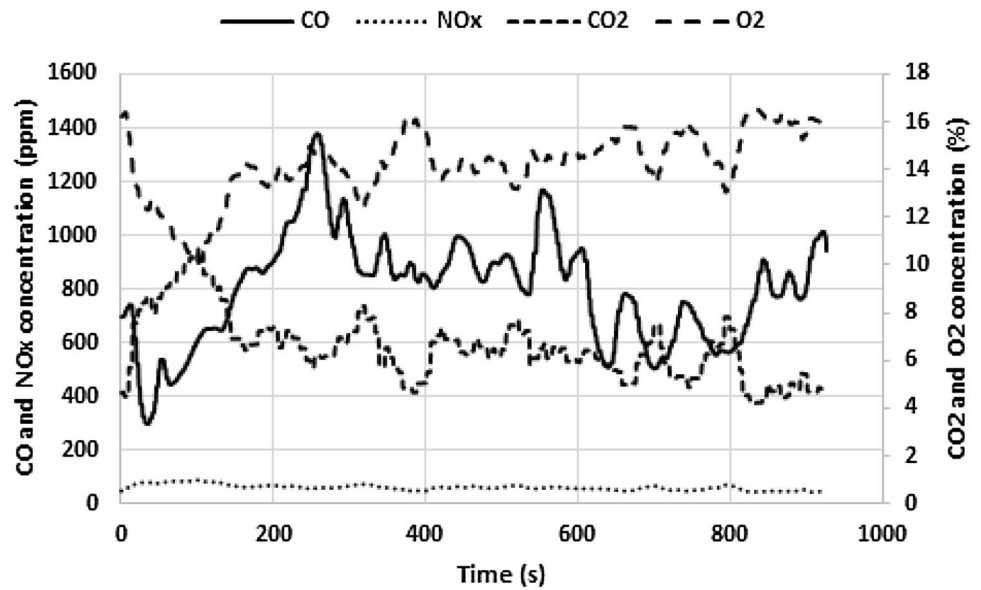
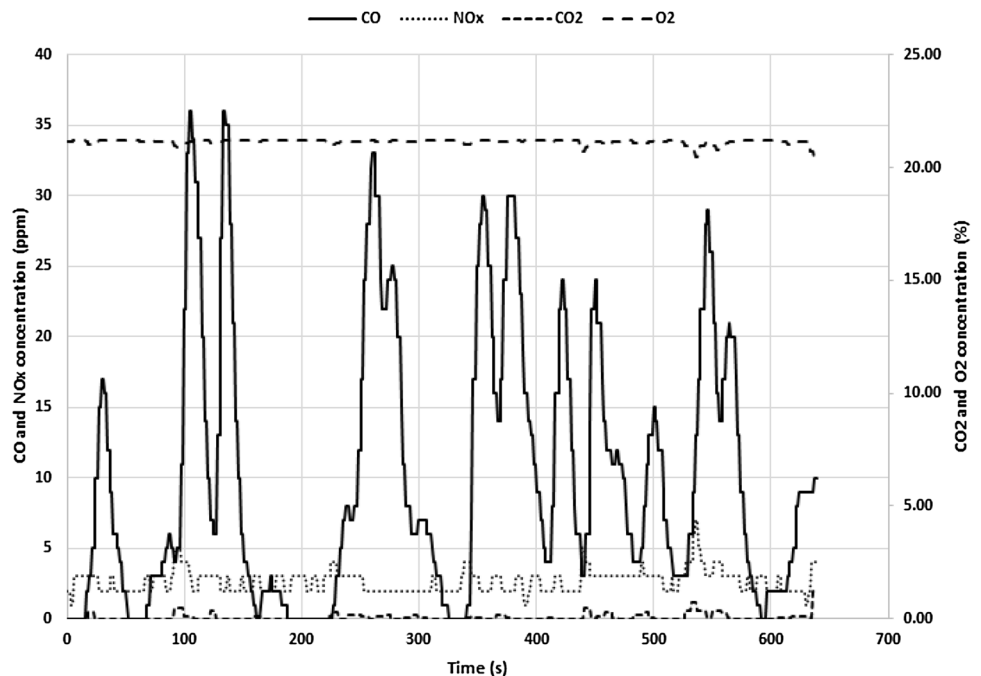


Fig. 7 Gases concentrations measured in the fume exhaust: CO (solid line, ppm), NOx (dotted line, ppm), CO₂ (small hyphened line, %) and O₂ (large hyphened line, %)



behavior, especially its draught, the combustible, and its introduction in the stove.

3.3 Gaseous emissions measured during a water ebullition test with the ring configuration

The main pollutant gases (CO, CO₂ and NOx), together with O₂, were continuously measured in the center of the combustion zone, Fig. 6, in the fume exhaust, Fig. 7, 20 cm above the tube allowing the pellet injection, Fig. 8, and 50 cm above the top of the system, Fig. 9. The

concentrations were measured in ppm for CO and NOx (principal axis) and in percentages for CO₂ and O₂ (secondary axis).

In Fig. 6, the O₂ emissions are approximately equal to 15%, whatever the time. The missing 6% are being used for the combustion and produce CO₂, or CO if the combustion is incomplete.

When the gases are collected in the combustion zone, the CO concentration varies between 300 and 1400 ppm, with a mean value equal to 684 ppm. The CO emissions highly oscillate, as they depend on the combustion behavior, see the previous comments on this combustion

Fig. 8 Gases concentrations measured 20 cm above the tube: CO (solid line, ppm), NO_x (dotted line, ppm), CO₂ (small hyphened line, %) and O₂ (large hyphened line, %)

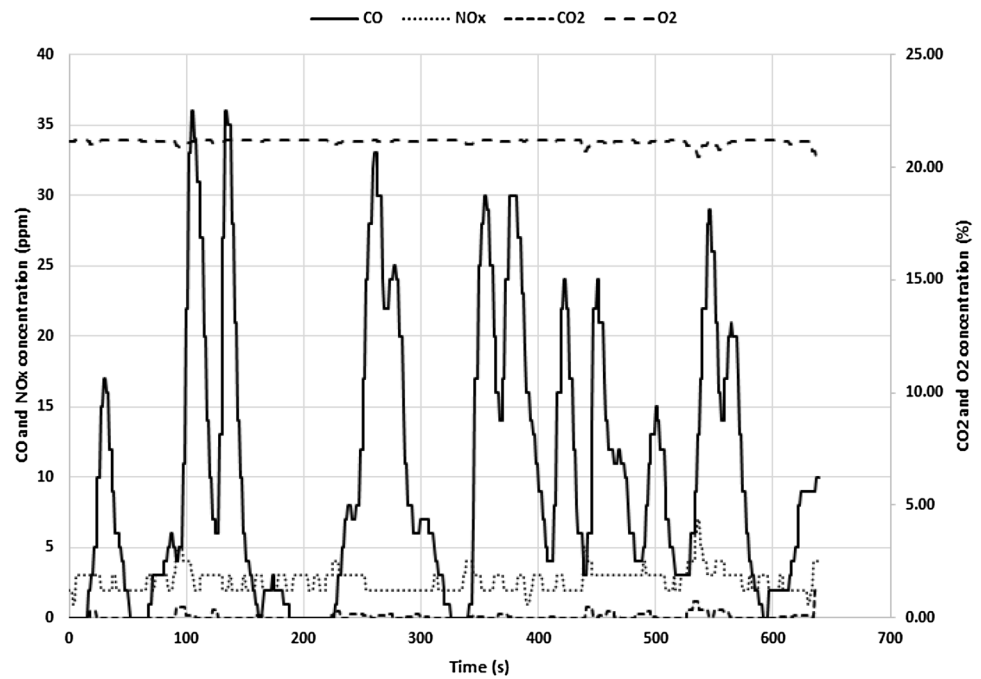
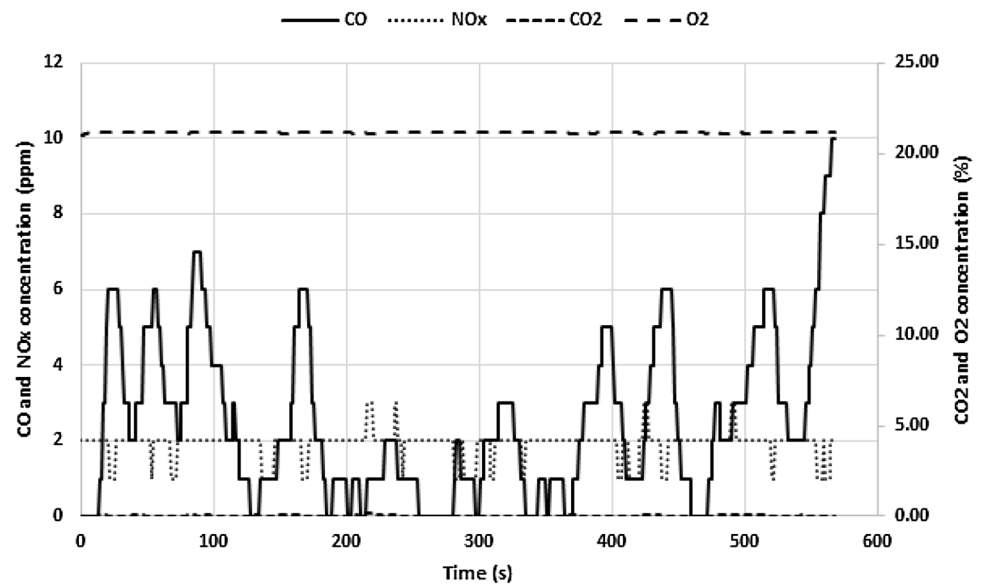


Fig. 9 Gases concentrations measured 50 cm above the plate: CO (solid line, ppm), NO_x (dotted line, ppm), CO₂ (small hyphened line, %) and O₂ (large hyphened line, %)



behavior. To minimize the CO emissions, it should be necessary to inject pellets in the combustion zone in a more regular way and with an adequate quantity. The CO₂ emissions oscillate between 4 and 8%, with a mean value equal to 6.35%.

Figures 7–9 show that the CO concentrations measured outside the cookstove highly oscillate probably due to wind, as the water ebullition tests were performed outside, and even in a zone sheltered from wind. These CO concentrations are higher at the cookstove exit, Fig. 7. At human height, Fig. 10, these CO concentrations vary between 0

and 7 ppm, which is very low. For reference, the maximal CO concentrations suggested by WHO depend on the time exposure and are equal to 5 ppm during 24 h, 9 ppm during 8 h, 32 ppm during 1 h, and 90 ppm for 15 min, [29], these thresholds being revised in 2020.

The NO_x concentrations are negligible, whatever the measurement point “far” from the combustion zone. This is usual for biomass combustion, as the N amount in the pellet is low, see Table 1.

The O₂ concentration remains stable at approximately 21% whatever the measurement point above the

combustion zone. This may be the consequence of a fast mixing with outside air.

Few papers analyzed the gases and particulate matter present in Sub-Saharan houses when burning tropical wood residue in a domestic stove, being the three-stone-fire type the most common in Sub-Saharan countries [13, 26], and [7]. For example, the CO concentration was measured in homes equipped with a three-stone-fire stove at 29.5 ppm (47 mg/Nm³) in [26]. The gases concentrations are analyzed in [30] during the combustion of Douglas fir in different stoves similar to that which can be used in Cameroon using a portable monitoring emission system from APROVECHO. The CO concentrations collected during the whole combustion experiment were measured between 17 and 85 g, depending on the stove and on the fuel moisture. In [24], mean 24 h indoor CO concentrations were measured between 15

and 62 ppm in Uganda kitchens after charcoal combustion performed in open fire stoves.

3.4 Simulations deduced from the heat transfer models

3.4.1 Simulation of the plate temperature during a combustion test and determination of the optimal convection coefficients h_i and $h_{e,pl}$

When solving the differential Eq. (5) with Scilab software, the optimal values of the convection coefficients are found equal to $h_i = 31.2 \text{ W.m}^{-2}.K^{-1}$ and $h_{e,pl} = 7.9 \text{ W.m}^{-2}.K^{-1}$. The experimental and simulated plate temperatures are presented in Fig. 10 versus time, along the combustion test.

Fig. 10 Experimental (solid line) and simulated (dotted line) plate temperature along the combustion experiment with the plate configuration

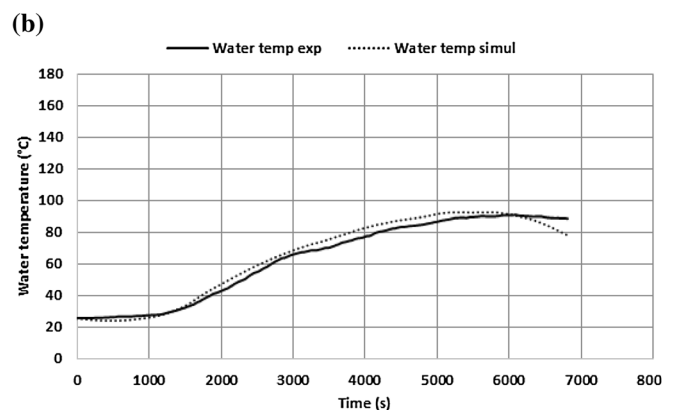
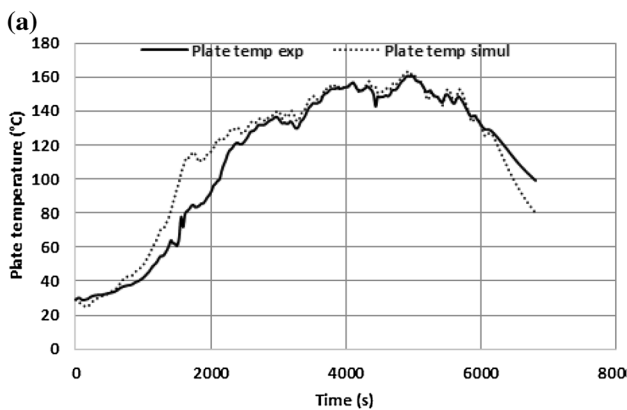
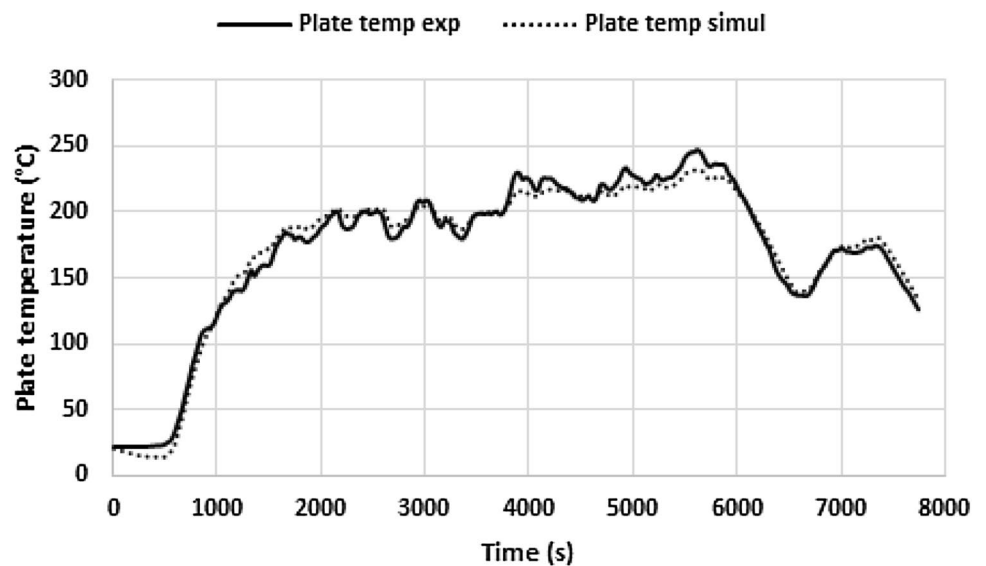


Fig. 11 Experimental (solid line) and simulated (dotted line) plate a) and water b) temperatures during a water ebullition test, in the plate configuration

The model quite perfectly simulates the plate temperature along the combustion test. The maximal difference between the experimental and simulated plate temperatures is equal to 15.5 °C, which represents a relative difference equal to 7%.

Among the four terms present between parentheses in the right-hand side of the differential Eq. (5), the fourth one is largely preponderant with values higher than 5.0×10^5 W. The other terms of this right-hand side take values always lower than 0.3 W, and the second term is the smallest one with values lower than 5.0×10^{-3} W. Changing the value of the flame emissivity in this second term does not significantly change the result.

3.4.2 Simulations of the plate and water temperatures during a water ebullition test in the configuration with a plate

Simulations of the plate and water temperatures during a water ebullition test with the plate configuration were realized, through the resolution of the system (9)-(10). Figure 11 gathers these experimental and simulated plate and water temperatures.

In this plate configuration, the optimal values of the parameters are: $k_e = 196.7 \text{ W.m}^{-2}.\text{K}^{-1}$, $h_{e,h} = 52.6 \text{ W.m}^{-2}.\text{K}^{-1}$, and $h_{e,v} = 11.3 \text{ W.m}^{-2}.\text{K}^{-1}$. The maximal difference between the experimental and simulated temperatures is equal to 34.8 and 10.7 °C for the plate and water respectively, whence a relative maximal difference equal to 21.8 and 11.3%, respectively. The model tends to overestimate the plate temperature at the beginning of the water ebullition test. The water temperature is simulated in much better way. Again the term $F_{b,pl}\epsilon_{fl}S_b\sigma T_{fl}^4(t)$ which appears in (9)-(10) does not bring a significant contribution to the evolution of the plate temperature, being

much lower than the other terms present in these balance equations.

3.4.3 Simulations of the water temperature during a water ebullition test in the configuration with a ring

The resolution of the system (14)-(15) of differential equations leads to the optimal values of the parameters k_e , $h_{e,r}$, h_i , $h_{e,hr}$, and $h_{e,v}$ respectively equal to $k_e = 38.1 \text{ W.m}^{-2}.\text{K}^{-1}$, $h_{e,r} = 57.5 \text{ W.m}^{-2}.\text{K}^{-1}$, $h_i = 29.6 \text{ W.m}^{-2}.\text{K}^{-1}$, $h_{e,h} = 8.8 \text{ W.m}^{-2}.\text{K}^{-1}$, and $h_{e,v} = 45.0 \text{ W.m}^{-2}.\text{K}^{-1}$. These values are different from the ones obtained in the plate configuration, due to the configuration change. In [22], the authors took convection coefficients between 14 and $45 \text{ W.m}^{-2}.\text{K}^{-1}$, depending on the cookstove.

Figure 12 gathers the experimental and simulated ring and water temperatures.

The maximal difference between the experimental and simulated ring temperatures is equal to 23.0 °C, leading to a maximal relative difference equal to 9.2%. The model here tends to underestimate the ring temperature in the intermediate stage and to overestimate it at the end of the test. The model slightly overestimates the water temperature at the beginning of the water ebullition test, in the fast increase stage. Then the experimental and simulated water temperature curves cross at approximately 5000 s. Nevertheless, the experimental temperature is quite well simulated. The maximal difference between the experimental and simulated water temperatures is equal to 8.3 °C, leading to a maximal relative difference equal to 8.2%.

In the different tests and configurations, the heat transfer models return quite satisfying simulations of the plate, or ring, and water temperatures. The values of the convection coefficients can be accepted, as the simulations quite well reproduce the tests.

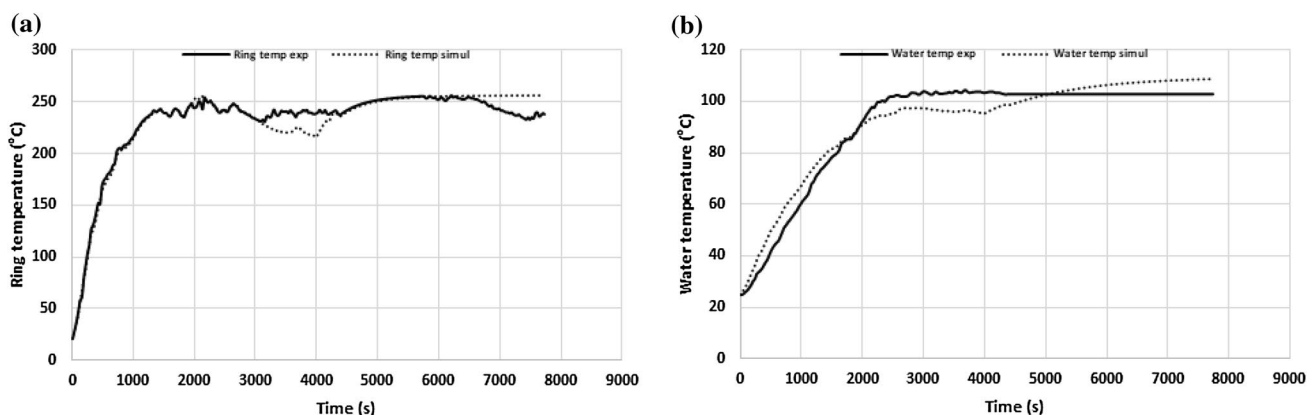


Fig. 12 Experimental (solid) and simulated (dotted) ring a) and water b) temperatures along a water ebullition test, in the configuration with a ring

3.5 Cookstove power and yield, and solid fuel consumption

As already indicated, the pellet injection was approximately equal to 10 pellets every 30 s, leading to a mass flow of $0.9/3600 \text{ kg}\cdot\text{s}^{-1}$. From the LHV value given in Table 1, the cookstove power may be computed through (17) as:

$$P_{tot} = \frac{0.9}{3600} \times 17.3 \times 10^6 = 4336 \text{ W}.$$

With standard deviations of the LHV computation evaluated at $90 \text{ kJ}\cdot\text{kg}^{-1}$, the cookstove power is equal to $4336 \pm 23 \text{ W}$.

Combustion and water ebullition tests were performed burning different biomass in six traditional or improved cookstoves in [13]. The power of a traditional charcoal stove was evaluated at 4.2 kW, that of a three-stone stove was here evaluated at 7.3 kW and that of improved stoves between 3.0 and 4.8 kW. The power of a mud stove with grate, a mud stove no grate and a three-stone open fire stove were evaluated in [19] at 7.72, 8.08 and 8.00 kW, respectively.

As described in Sect. 2.7, different components of this overall power may be evaluated using mean values of the temperatures or concentrations which are involved.

The power associated with the upwards radiation of the burner is computed through (18) as: $P_{r,b} = 766 \pm 6 \text{ W}$.

The power associated with the downwards radiation from the ashtray is computed through (19): $P_{r,a} = 336 \pm 3 \text{ W}$.

The mean value of the fume temperature is $T_{fu} = 150.0 \text{ }^\circ\text{C}$. The power associated with the sensitive heat losses in the fume is computed through (20):

$$P_{fu,s} = 1794 \pm 16 \text{ W}.$$

The power associated with the latent heat losses in the fume is computed through (21): $P_{fu,l} = 118 \pm 9 \text{ W}$.

The heat losses in the fume ($1912 \pm 25 \text{ W}$) represent 44% of the power P_{tot} supplied by the pellet combustion. Nevertheless, part of this power is transferred to the ring or water, as the fume flow outside the cookstove while licking the ring and pot.

Recalling the time required for the water to reach $100 \text{ }^\circ\text{C}$ equal to 2310 s, see Fig. 5, the mass of pellets burnt during this time length is equal to $0.9 \frac{2310}{3600} = 0.578 \text{ kg}$. From (24), the cookstove yield is computed as: $\eta = 12.3 \pm 0.1\%$, which seems a low value.

The specific fuel consumption is equal to $0.12 \text{ kg}_{combustible}/\text{kg}_{water}$.

The actual specific dry and wet flue gas volume respectively defined in (25) and (26) are equal to $G_d = 12.6 \text{ Nm}^3\cdot\text{kg}^{-1} \text{ fuel}$, $G_w = 13.3 \text{ Nm}^3\cdot\text{kg}^{-1} \text{ fuel}$.

For comparison, the thermal efficiency of a traditional charcoal stove was evaluated at 21% in [13], the authors indicating a thermal efficiency of 17% for a three-stone stove and a thermal efficiency lying between 17 and 26% for three improved cookstoves. In [6], the efficiency of a top-lit up-draught gasifier cooking stove was computed between 14 and 34%, depending on the combustible (corn cobs, wood chips or peanut shell pellets) and the fuel load. The thermal efficiency of a stove assembled by Philipps with natural draught was measured at 24% in [8]. In [9], the efficiency of three improved cookstoves were evaluated between 11.6 and 18.0%, for water ebullition tests under cold start, like in the present study. In [10], the thermal efficiency was evaluated between 21 and 32% for a cold-start water ebullition test in an improved biomass stove burning charcoal produced from Neem tree (*Azadirachta indica*) or Indian Lilac. In [22], the authors evaluated the yield of their shielded fire household cookstoves between 35.8 and 36%, depending on the humidity of the fuel. The stove yield was evaluated between 11.7 and 19% for cold-start water ebullition tests in [19]. The yield of three-stone stoves was evaluated at 17% and at 25% in [7] for an appliance using wood combustion under a tripod stand. The present stove yield is close to that of the rudimentary three-stone one. One reason for the low value of the cookstove yield considered in the present study is that 67% of the power produced from the pellet combustion is lost in the fume. In [31], the cookstove efficiency was evaluated between 13 and 26% for a Chinese top-lit up-draught biomass semi-gasifier cooking stove, during fuel combustion. In [33], the thermal efficiency was evaluated between 10 and 15% for wood combustion in a Chinese stove without a chimney burning cotton stalk, peanut shell, or corn stover.

In [13], the time to ebullition was measured between 12 and 42 min, for different cookstoves and different combustibles. In [19], this time to ebullition was evaluated between 17 and 22 min, for cold start in a mud stove with grate, a mud stove no grate and a three-stone open fire stove.

In [19], the specific fuel consumption of a mud stove with grate, a mud stove no grate and a three-stone open fire stove were evaluated at 227.44, 219.44 and 225.42 $\text{g}\cdot\text{L}^{-1}$, respectively. In [9], the specific consumption of three improved cookstoves were measured between 169 and 261 $\text{g}\cdot\text{L}^{-1}$. The specific fuel consumption was evaluated in [14] at 85 $\text{g}\cdot\text{L}^{-1}$ for a coal start water ebullition test in different biomass cookstove. The CO concentrations were measured between 7 and 20 ppm and the thermal efficiency

between 14 and 29%, depending on the stove. The influence of different parameters on the efficiency of a water ebullition test was analyzed in [25].

The quite high differences observed in the literature for the cookstove powers, yields, times to ebullition... may result of the significant differences in the conception of the cookstoves, in the experiments and in the combustibles which were used for the combustion or water ebullition tests.

4 Conclusion

A low-cost prototype of improved pellet cookstove was manufactured. Combustion tests were performed with standardized EN+ pellets with a thick steel plate on the upper part of the cookstove. Water ebullition tests were performed with two configurations: a thick steel plate or a thick steel ring on the upper part of the cookstove. The water temperature of 100 °C was only reached with the ring configuration. The temperatures and main gases concentrations were measured at different points of the system. Simple and phenomenological models of the thermal behavior were proposed and simulations of the plate, or ring, and water temperatures were obtained in the three configurations with quite good agreement, the relative maximal differences between the experimental and simulated temperatures being equal to 7 or 21%. The convection coefficients involved in these models were determined through the resolution of the balance equations and comparing the experimental and simulated temperatures. For the water ebullition tests, the cookstove yield was evaluated at $12.3 \pm 0.1\%$, which is slightly lower than the results from the literature, because the heat losses are very high in the fume. Further improvements of this prototype will be considered, especially concerning the shape of the combustion zone to reduce the heat losses in the fume (44% of the cookstove power). An automatic pellet injection through an auger screw will also be considered to reduce the combustion perturbations, leading to high oscillations of the grid temperature along the test. Combustion tests performed with local woody residue or biomass should also be performed to proceed in a circular economy, which could further reduce the deforestation in Sub-Saharan countries. An economic assessment of such an improved pellet cookstove should finally be performed like in [20], as the purpose is to envisage a favorable commercial distribution of such cookstove in Cameroon and, more generally, in Sub-Saharan countries.

Acknowledgements The authors thank Prof. Gwenaëlle Trouvé (LGRE, UHA), for stimulating discussions concerning the study.

Declarations

Conflict of interest The authors declare that there are no conflicts of interests regarding the publication of this paper.

Transparency The authors confirm that the manuscript is an honest, accurate, and transparent account of the study was reported; that no vital features of the study have been omitted; and that any discrepancies from the study as planned have been explained.

Ethical approval This study follows all ethical practices during writing.

Open Access This article is licensed under a Creative Commons Attribution 4.0 International License, which permits use, sharing, adaptation, distribution and reproduction in any medium or format, as long as you give appropriate credit to the original author(s) and the source, provide a link to the Creative Commons licence, and indicate if changes were made. The images or other third party material in this article are included in the article's Creative Commons licence, unless indicated otherwise in a credit line to the material. If material is not included in the article's Creative Commons licence and your intended use is not permitted by statutory regulation or exceeds the permitted use, you will need to obtain permission directly from the copyright holder. To view a copy of this licence, visit <http://creativecommons.org/licenses/by/4.0/>.

References

1. Afnor (2006) Solid mineral fuels - Determination of sulfur by IR spectroscopy. ISO 19579:2006 October 2006
2. Afnor (2010) Solid mineral fuels - Determination of total carbon, hydrogen and nitrogen content - Instrumental method. ISO 29541:2010 October 2010
3. Afnor (2014) Solid biofuels - Fuel specifications and classes - Part 2 : graded wood pellets. NF EN ISO 17225-2 June 2014
4. Afnor (2015) Solid biofuels - Determination of ash content. NF EN ISO 18122 December 2015
5. Afnor Residential solid fuel burning appliances - Part 1 : general requirements and test methods. NF EN 16510-1 July 2018
6. Ahmad R, Zhou Y, Zhao N, Abbas A, Li G, Perumal R, Pemberton-Pigott C, Sultan M, Dong R (2018) Performance of top-lift updraft gasifier stove using different biomass fuels. *Fresenius Environ Bull* 28:9835–9842
7. Anozie A, Bakare A, Sonibare J, Oyebisi T (2007) Evaluation of cooking energy cost, efficiency, impact on air pollution and policy in Nigeria. *Energy* 32:1283–1290. <https://doi.org/10.1016/j.energy.2006.07.004>
8. Arora P, Das P, Jain S, Kishore VVN (2014) A laboratory based comparative study of Indian biomass cookstove testing protocol and Water Boiling Test. *Energy Sustain Dev* 21:81–88. <https://doi.org/10.1016/j.esd.2014.06.001>
9. Bailis R, Berrueta V, Chengappa C, Dutta K, Edwards R, Masera O, Still D, Smith KR (2007) Performance testing for monitoring improved biomass stove interventions: experiences of the Household Energy and Health Project. *Energy Sustain Dev* 11:57–70. [https://doi.org/10.1016/S0973-0826\(08\)60400-7](https://doi.org/10.1016/S0973-0826(08)60400-7)
10. Boafo-Mensah G, Darkwa KM, Laryea G (2020) Effect of combustion chamber material on the performance of an improved biomass cookstove. *Case Stud Therm Eng* 21:100688. <https://doi.org/10.1016/j.csite.2020.100688>

11. Carvalho L, Wopienka E, Pointner C, Lundgren J, Verma VK, Haslinger W, Schmidl C (2013) Performance of a pellet boiler fired with agricultural fuels. *Appl Energy* 104:286–296. <https://doi.org/10.1016/j.apenergy.2012.10.058>
12. D05 Committee Practice for Ultimate Analysis of Coal and Coke. ASTM D3176 - 15. ASTM International
13. Grimsby LK, Rajabu HM, Treiber MU (2016) Multiple biomass fuels and improved cook stoves from Tanzania assessed with the Water Boiling Test. *Sustain Energy Technol Assess* 14:63–73. <https://doi.org/10.1016/j.seta.2016.01.004>
14. Gupta A, Mulukutla ANV, Gautam S, TaneKhan W, Waghmare SS, Labhasetwar NK (2020) Development of a practical evaluation approach of a typical biomass cookstove. *Environ Technol Innov* 17:100613. <https://doi.org/10.1016/j.eti.2020.100613>
15. Jagger P, Das I (2018) Implementation and scale-up of a biomass pellet and improved cookstove enterprise in Rwanda. *Energy Sustain Dev* 46:32–41. <https://doi.org/10.1016/j.esd.2018.06.005>
16. Jannot Y, Moynes C (2016) Transferts thermiques: cours et 55 exercices corrigés. Éditions, Saint-Denis. ISBN 978-2-332-83699-1
17. Kenfack J, Lewetchou KJ, Bossou OV, Tchaptchet E (2017) How can we promote renewable energy and energy efficiency in Central Africa? A Cameroon case study. *Renew Sustain Energy Rev* 75:1217–1224. <https://doi.org/10.1016/j.rser.2016.11.108>
18. Kshirsagar MP, Kalamkar VR (2014) A comprehensive review on biomass cookstoves and a systematic approach for modern cookstove design. *Renew Sustain Energy Rev* 30:580–603. <https://doi.org/10.1016/j.rser.2013.10.039>
19. Kuhe A, Iortyer HA, Iortsor A (2014) Performance of Clay Wood Cook Stove: An Analysis of Cost and Fuel Savings. *J Technol Innov Renew Energy* 3:94–98. <https://doi.org/10.6000/1929-6002.2014.03.03.2>
20. Kumar H, Panwar NL (2019) Experimental investigation on energy-efficient twin-mode biomass improved cookstove. *SN Appl Sci* 1:760. <https://doi.org/10.1007/s42452-019-0804-x>
21. Lombardi F, Riva F, Bonamini G, Barbieri J, Colombo E (2017) Laboratory protocols for testing of improved cooking stoves (ICSs): a review of state-of-the-art and further developments. *Biomass Bioenergy* 98:321–335. <https://doi.org/10.1016/j.biombioe.2017.02.005>
22. MacCarty NA, Bryden KM (2016) A generalized heat-transfer model for shielded-fire household cookstoves. *Energy Sustain Dev* 33:96–107. <https://doi.org/10.1016/j.esd.2016.03.003>
23. Mehrete SA, Panwar NL, Sharma D, Kumar H (2017) Improved biomass cookstoves for sustainable development: a review. *Renew Sustain Energy Rev* 73:672–687. <https://doi.org/10.1016/j.rser.2017.01.150>
24. Nakora N, Byamugisha D, Birungi G (2020) Indoor air quality in rural Southwestern Uganda: particulate matter, heavy metals and carbon monoxide in kitchens using charcoal fuel in Mbarara Municipality. *SN Appl Sci* 2:2037. <https://doi.org/10.1007/s42452-020-03800-0>
25. Quist CM, Jones MR, Lewis RS (2020) Influence of variability in testing parameters on cookstove performance metrics based on the water boiling test. *Energy Sustain Dev* 58:112–118. <https://doi.org/10.1016/j.esd.2020.07.006>
26. Tumwesige V, Okello G, Semple S, Smith J (2017) Impact of partial fuel switch on household air pollutants in sub-Saharan Africa. *Environ Pollut* 231:1021–1029. <https://doi.org/10.1016/j.envpol.2017.08.118>
27. Van Krevelen DW, Te Nijenhuis K (2009) Properties of Polymers Their Correlation with Chemical Structure; their Numerical Estimation and Prediction from Additive Group Contributions. Elsevier Science & Technology Books, Amsterdam, Netherlands
28. Verma VK, Bram S, Gauthier G, De Ruyck J (2011) Evaluation of the performance of a multi-fuel domestic boiler with respect to the existing European standard and quality labels: Part-1. *Biomass Bioenergy* 35:80–89. <https://doi.org/10.1016/j.biombioe.2010.08.028>
29. World Health Organization (2018) Air pollution and child health. Prescribing clean air. <https://www.who.int/ceh/publications/air-pollution-child-health/en/>. Accessed 8 Aug 2020
30. Yuntenwi E (2008) Improved biomass cookstoves - A strategy towards mitigating indoor air pollution and deforestation. A case study of the North West province of Cameroon. PHD Dissertation, Cottbus University. https://opus4.kobv.de/opus4-btu/files/420/diss_ernestine_pdf.pdf. Accessed 7 Aug 2020
31. Zhang Y, Zhang Z, Zhou Y, Dong R (2018) The influences of various testing conditions on the evaluation of household biomass pellet fuel combustion. *Energies* 11:1131. <https://doi.org/10.3390/en11051131>
32. Zhang Z, Zhang Y, Zhou Y, Ahmad R, Pemberton-Pigott C, Annegarn H, Dong R (2017) Systematic and conceptual errors in standards and protocols for thermal performance of biomass stoves. *Renew Sustain Energy Rev* 72:1343–1354. <https://doi.org/10.1016/j.rser.2016.10.037>
33. Zongxi Z, Zhenfeng S, Yinghua Z, Hongyan D, Yuguang Z, Yixiang Z, Ahmad R, Pemberton-Pigott C, Renjie D (2017) Effects of biomass pellet composition on the thermal and emissions performances of a TLUD cooking stove. *Int J Agric Biol Eng* 10:189–197. <https://doi.org/10.25165/j.ijabe.20171004.2963>

Publisher's Note Springer Nature remains neutral with regard to jurisdictional claims in published maps and institutional affiliations.